Statistical and Experimental Analysis of Process Parameters of 3D Nylon Printed Parts by Fused Deposition Modeling: Response Surface Modeling and Optimization

Moradi, M., Aminzadeh, A., Rahmatabadi, D. & Rasouli, A.

Moradi, M, Aminzadeh, A, Rahmatabadi, D & Rasouli, A 2021, 'Statistical and Experimental Analysis of Process Parameters of 3D Nylon Printed Parts by Fused Deposition Modeling: Response Surface Modeling and Optimization', *Journal of Materials Engineering and Performance*, vol. 30, no. 7, pp. 5441-5454.
https://doi.org/10.1007/s11665-021-05848-4

Original citation & hyperlink:

DOI 10.1007/s11665-021-05848-4
ISSN 1059-9495
ESSN 1544-1024

Publisher: Springer

The final publication is available at Springer via http://dx.doi.org/10.1007/s11665-021-05848-4

Statistical and experimental analysis of process parameters of 3D Nylon Printed Parts by Fused Deposition Modelling; Response Surface Modelling and Optimization

Mahmoud Moradi[1], Ahmad Aminzadeh [2], Davood Rahmatabadi[4] S.A.Rasouli[*3],

1- *School of Mechanical, Aerospace and Automotive Engineering, Faculty of Engineering, Environment and Computing, Coventry University, Coventry, UK*

2- *Department of Mathematics, Computer Science and Engineering, Université du Québec à Rimouski, Rimouski, Québec, Canada*

3- *Department of Mechanical Engineering, Faculty of Engineering, Malayer University, Malayer, Iran*

4- *School of Mechanical Engineering, College of Engineering, University of Tehran, Tehran, Iran*

Abstract

In the current study, the additive manufacturing of nylon by fused deposition modeling (FDM) is conducted based on statistical analysis. Besides, the aim of this study is the influence of process parameters, namely layer thickness (0.15 mm - 0.35mm), infill percentage (15 % - 55 %), and the number of contours (2 - 6) on the maximum failure load, parts weight, elongation at break, and build time. The experiment (DOE) approach was used to optimize process parameters based on the statistical evaluates to reach the best objective function. The minimum value of build time and maximize of the failure load was considered as objective functions. The response surface method (RSM) is regarded as an optimization process parameter and optimum conditions were studied by experimental research to evaluate efficiency. Based on the results, the layer thickness is the significant primary variable for all responses. The experimental evaluation showed that the maximum values of failure load and elongation were obtained by changing the layer thickness from the lowest to the highest. By reduction in layer thickness at the same printing speed, the cooling rate increases, which results in greater strength and less elongation. As a result, it could be concluded that by increasing the number of contour layers from 2 to 6, the maximum failure force increased 42%. Increasing the contours due to the similar effect to increasing the infill density, increases the failure force and production time, which is also confirmed by the ANOVA.

Keywords: Additive Manufacturing; Fused Deposition Modelling (FDM); Mechanical properties; Nylon; Response Surface Method (RSM).

1. Introduction

A rapid manufacturing system or 3D printing has been considered a new production method several decades ago. This technique currently revolutionizes the commercial engineering sector specially for polymer manufacturing and goals to substitute the traditional methods. In combination with novel material technologies, additive manufacturing (AM) plays a vital role in economic competitiveness [1]. In this regard, 3D printing regarding AM enables technology for a wide range of new polymer products [2,3]. Nowadays, modern manufacturing companies become encouraged to applying several AM techniques in their productions, such as Laminated Object Manufacturing (LOM) [4], Stereo-lithography (SLA) [5], Selective Laser Sintering (SLS) [6], Selective Laser Melting (SLM) [7], Direct Metal Laser Sintering (DMLS) [8], 3D printing (3DP) [9], Fused Deposition Modeling (FDM) [10]. Overall, all these AM methods employ the same basic principle wherein the final part is made-up with layer by layer [2]. The concept of AM is the recent move into intelligent technology in several industries. However, more recently, there have been developments in the biomedical manufacturing system (Custom made), including aerospace, automotive, dental, food production systems, and constructions [11]. All in all, due to rapid processing, ease of handling, simplicity, and cost-efficiency, Fused deposition modeling (FDM) is the most commonly used 3D printing method for thermoplastics materials [12,13].

With the growth of 3D printing methods, for the production of polymer parts, there is an attractive dilemma for choosing the production method between injection molding and 3D printing. But there are parameters that can make this choice easier. These parameters are mechanical properties, number of samples, geometric complexity, dimensions, cost and surface roughness. Injected samples usually have higher mechanical properties and, more importantly, isotropic properties, and due to the high cost of the mold, it is usually suitable for high circulation. On the other hand,

the production of parts with special geometries, small dimensions at a very low cost is possible using the 3D printing method. Fused deposition modeling (FDM), also known as fused filament fabrication (FFF), is a simple AM technology. The filament is extruded through a nozzle that melts while being gradually deposited in a structured way on the build platform until the object is finished [14,15]. Furthermore, injection molding as a polymer production method has other limitations, such as part design restrictions, high initial tooling cost, and complex fabrication approaches [16].

The current levels of researches and developments in polymers such as ABS [17–19], PLA [20–23], polyamide [24,25], high-density polyethylene (HDPE) [26], polycarbonate (PC) [27], and polyurethane (PU) [28] are manufactured using FDM have generated extra opportunities for discovering potential applications for AM/3DP techniques. In contrast, strong dependence of properties on printing parameters has made it a major subject of researches in this field, despite the passage of several years. On the other hand, polymer products fabricated using FDM have not proper strength and adhesion due to voids caused by incomplete diffusion at the interfaces during fabrication and researchers are looking to find the optimal parameters to solve this constraint. Some of these researches are listed in Table 1 with presenting the investigated printing parameters, design of experiment (DOE) methods and used materials.

In the meantime, the use of new materials with suitable properties accelerates to find the optimal FDM printing parameters. Although, as mentioned, a lot of researches have been done in the field of FDM, but nylon has not been considered very well and with its extraordinary properties, it can be used in industrial applications and can replace ABS, as the most widely used filament used in FDM, even at a much lower price [29]. In the past, nylon use was limited to textiles, but today, due to its high strength, there are more applications, including for the manufacture of parts

in the automotive industry (such as gears, fittings, bearings). Nylon is the best candidate for gears, fan blades, sprockets, latches, manifolds, and bearing surfaces because these materials are self-lubricating, very wear-resistant, and thermally firm. Additionally, nylon is very light, with 15% steel and 40% of aluminum. One of the most critical factors affecting the mechanical, metallurgical, and physical properties and surface quality is the filament material properties. Several studies have concentrated on studying the impact of process parameters on input response and to determine optimal conditions during FDM process for nylon. Zhang et al. [24] evaluated the wear and thermal characteristics of 3D printed using nylon 618, nylon 645, alloy 910 filaments to produce nylon spur gears. According to the results, nylon 618 provided the best wear performance. Sunny et al. [30] used numerical comparison approaches for fluid-structure interaction simulation of FDM nylon parts. More recently, Singh et al. [31] have looked at the statistically controlled FDM solution-assisted nylon6-Al-Al2O3 replica-based IC procedure. A developed model to optimize different process parameters such as printing time, mechanical properties, and volume prediction in printing configuration by Taguchi's prediction model was presented by Mostafa et al. [32].

In general, the printing parameters are in three categories of structural parameters, extruder geometry and process parameters, which are in the category of process parameters of nozzle temperature and bed, printing speed, etc., and usually according to the filament, the manufacturer proposes the optimal value. Also, nozzle parameters also include the diameter of the nozzle, which according to the required accuracy, sample dimensions and surface smoothness, different diameters are used. Of course, all these parameters have been studied extensively, but the most important part is the structural parameters, which have a great variety and despite much study, are still considered. These parameters include the direction, angle and pattern of printing and

arrangement of fibers, density, number of contours and thickness of layers, etc., and among these, the least attention is paid to the number of contours and its interaction and other parameters on mechanical properties which in this research has been selected for review.

Table1. Review of studies about FDM that used a statistical method

Author	Year	Parameter	Response	Method	Material
Moradi [33]	2020	focal plane position, laser power, and laser cutting speed	Geometrical features, kerf ratio	RSM	PLA
Nagendra [34]	2019	Layer thickness Print Temperature Raster Angle	Tensile strength Flexural strength	Taguchi	Nylon
Nagendra [35]	2019	Layer thickness temperature	Surface roughness Sliding force	Taguchi	Composite
Moradi [36]	2019	Layer thickness, infill percentage, and the extruder temperature	Maximum failure load Elongation at the break, part weight, and build time	RSM	Br-PLA
Rao [37]	2019	layer thickness, model tip diameter model build temperature	Tensile Strength	Full factorial	PLA
Moradi [22]	2019	Layer thickness, infill percentage, and the extruder temperature	Maximum failure load, elongation at the break, part weight	RSM	PLA
Nori Kamoon [38]	2018	Air gap Raster angle Build orientation	flexural strength	RSM	Nylon
Vishwas [39]	2018	Orientation Layer thickness shell thickness	ultimate tensile strength and dimensional	Taguchi	ABS and Nylon

Kumar Padhi [40]	2017	Layer thickness Raster angle Raster width	Length Width Thickness	Taguchi	ABS
Chaco [41]	2017	Build orientation Layer thickness Feed rate	Tensile and flexural strength	RSM	PLA

In this experimental research, to study the effects of layer thickness, infill percentage, number of contours, and their interactions on mechanical properties, build time, and part weight nylon tensile test sample was used. Also, the design of experiment (DOE) method was applied, and finally, Design-Expert^{TM} V8 software was exploited for statistical analysis of experimental data by response surface method (RSM). This study's objective function is to define the best process parameters and simultaneously controlled variables to produce tough nylon parts and reduce part weight and efficient conditions. The exploration was accomplished by RSM and verified by the experimental investigation, which in the statistical model was defined by getting the equivalent outcomes to experimental data.

2. Experimental Design and Methodology

2.1 Response Surface Method

In statistics science, Response surface methodology (RSM) gathers statistical techniques and mathematical for invention optimization between several explanatory variables [42,43]. RSM is usually applied together with a factorial design to reduce experimentation cost [44–48]. This method has a long history and nowadays has numerous applications in industrial and manufacturing [49,50]; it is specifically used in combination with finite element models. [51,52]. In general, in manufacturing and modeling uncertainty, the RSM is a good solution.

RSMs usually include the following stages:

- Experiments need to change the setting to the range of the functioning conditions where the response is optimum.
- The experiment needs to fit a more elaborate model between the response and the parameters in the optimum zone.
- Some responses may have to be optimized simultaneously.

In this current investigation, according to three input factors (layer thickness, infill percentage, number of contours and their interactions) and three output factors (mechanical properties, build time, and part weight), an experimental investigation was conducted to make some 3D models by using the RSM with least structure defects. Moreover, the statistical analysis was designed according to the central composite design (CCD) full replication with three factors on five levels. In that case, two-level FFD (Full Factorial Design) and a SED (Star Experimental Design**)** are combined simultaneously. This method can estimate the curvature of the design space. Regarding the approximation of the correct input-output function, the following polynomial models were used:

$$\eta = b_0 + \sum_{i=1}^{k} b_j X_j + \sum_{j=1}^{k} \sum_{i=1}^{k} b_{ij} X i X_i$$

Where b_0, b_j, and b_{ij} are the regression coefficients with i, j = 1, 2, …, k and Xi are the k input variables. Based on Table 2, levels of independent variables are adjusted. Coding reduces each factor's range to a standard scale, − 2 to + 2, regardless of its relative magnitude. According to the table 3, the designed experiments and results of experiments are shown.

Table 2. Levels of independent variables

Variable	**Symbol**	**Unit**	**Levels**				
			-2	**-1**	**0**	**1**	**2**
Layer Thickness	LT	mm	0.15	0.20	0.25	0.30	0.35

Infill Percentage	IP	%	15	25	35	45	55
Number of contours	NC	-	2	3	4	5	6

Table 3. Design matrix and experiments results

Run	Input Variables			Output Responses				
	Layer Thickness (LT)	**Infill Percentage (IP)**	**Number of contours (NC)**	**Failure Load (N)**	**Elongation at break (%)**	**Programed weigh(g)**	**Part Weight (g)**	**Build Time (min)**
1	0.30	25	3	171.7	517.8073	4.88	3.6	16
2	0.25	35	6	217.2	356.1583	5.78	4.2	22
3	0.25	35	4	134.9	113.1309	5.25	4.1	20
4	0.25	35	4	134.9	113.1309	5.25	4.1	20
5	0.25	15	4	202.3	261.4295	4.66	3.4	18
6	0.25	55	4	190.1	53.5331	5.89	4.3	21
7	0.20	45	5	533.4	162.0914	5.62	4	26
8	0.20	25	5	312.7	121.5711	5.00	3.6	24
9	0.20	45	3	128.8	155.9347	5.15	3.6	23
10	0.20	25	3	126.3	304.875	4.37	3.2	20
11	0.30	25	5	122.6	91.4716	5.39	4.1	17
12	0.25	35	4	134.9	113.1309	5.25	4.1	20
13	0.35	35	4	190.1	150.1418	5.94	4.4	16
14	0.30	45	5	363.5	595.9906	5.88	4.3	18
15	0.25	35	2	226.9	457.9961	4.82	3.4	18

1.2 Experimental Work

The nylon 12 filament prepared from YS company was used and its properties were presented according to Table 4. To better understand the printing parameters, each of them is first presented and defined in Table 5. Also, the values for fixed printing parameters are presented in Table 5. According to results of DOE (Table 3) and fixed printing parameters (Table 5), fifteen tensile test samples were designed and printed by the FDM with fully honeycomb pattern. The principle of FDM process by nylon filament and printing parameters description are shown in Figure 1. The simplify 3D software was applied to design and define material properties as build factors of samples. Uniaxial tensile test were printed according to ASTM-D 638 type-IV [53]. In Figure 2, dimensions of the tensile test sample according to ASTM-D638 type-IV and 3D printed samples are presented. Tensile test was performed at a speed of 1mm/min using Santam machine. The printed specimens have shells with 100% density and non-dense cores with different densities. So the number of contours is the same as the number of dense shells, and the infill density is the density of the core.

Table 4. Nylon filament properties.

Material Property	FDM Nylon
Elastic modulus, E (GPa)	0.493
Poisson's ratio	0.39
Ultimate tensile strength (MPa)	44.79
Yield stress (MPa)	3.61
Fracture toughness, (MPa m0.5)	0.92
Breaking strain (%)	16
Strain-hardening coefficient, k (MPa)	294.7138
Strain-hardening exponent, n (MPa)	0.8437
Fracture stress (MPa)	43.45

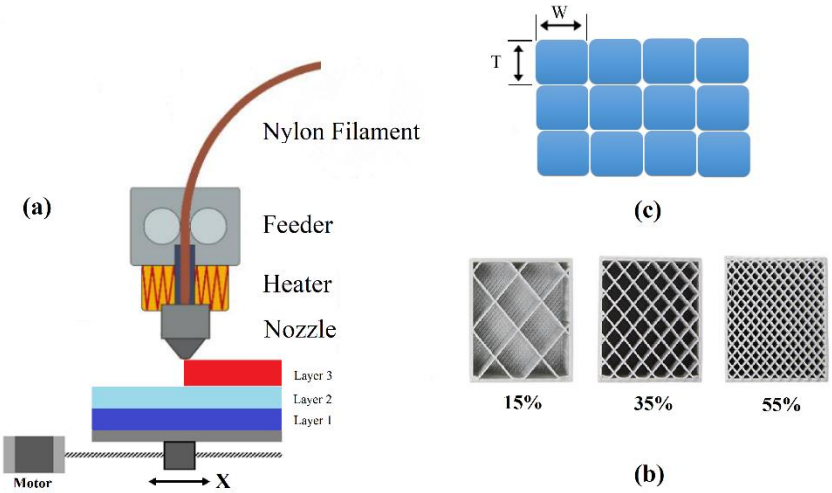

Figure 1. Principle of FDM process by Nylon filament and outputs description. a) Layer thickness, b) Infill percentage c) Number of contours

Table 5. FDM manufacturing parameters and values intended for fixed printing parameters

No	Build Parameters	Unit	Value	Definition
1	**Nozzle diameter**	**mm**	**0.45**	The diameter of the extruder nozzle.
2	**Extrusion width**	**mm**	**0.45**	The desired single-outline width of the plastic extrusion.
3	**Build orientation**	**Degree**	**45**	The angle between the central axis of the part and the horizontal direction.
4	**Top solid layer**	**-**	**6**	The number of solid layers required at the top of the part.
5	**Bottom solid layers**	**-**	**6**	Required number of solid layers at the bottom of the part.
6	**Default printing speed**	**mm/min**	**3600**	Initial speed used for all printing movements (modification may be added for cooling or outline underspeed).
7	**Retraction speed**	**mm/min**	**1800**	Extruder speed for the retraction movements typically uses the highest speed the extruder can support.
8	**Outline overlap**	**%**	**15**	Percentage of extrusion width that will overlap with outline perimeters (ensures infill bonds to outline).

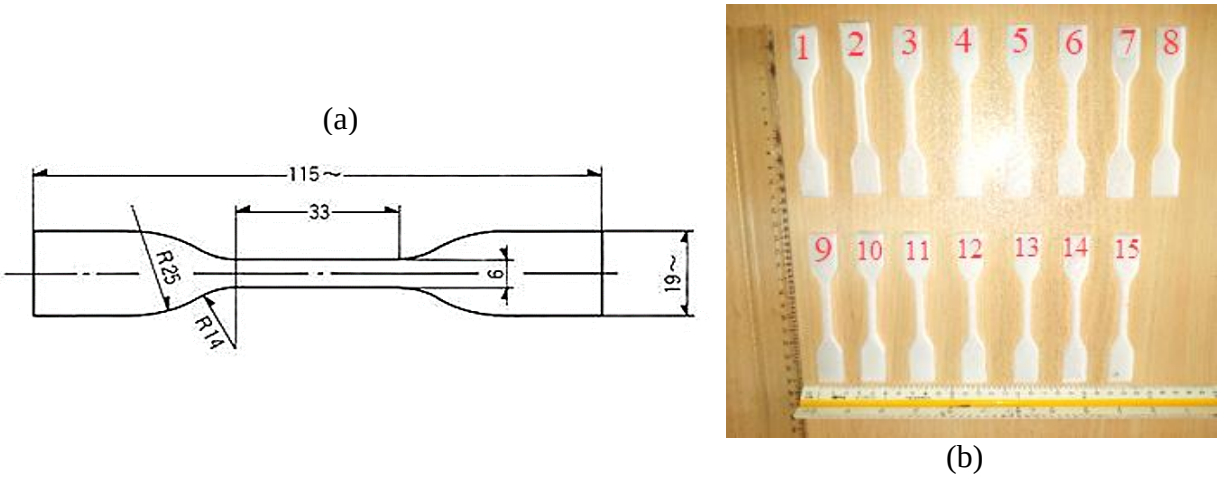

Figurer 2. Geometrical dimensions and set up of the sample. (**a**) dimensions of the tensile test sample according to ASTM-D638 type-IV and (**b**) 3D printed samples

On the other side, elongation at break (%), maximum failure load (N), part weight (g), and build time (min) opted as output responses. The measuring procedure was considered a standard condition. To this end, build time was calculated after printing each sample by a digital timer, and a precise weighing scale measured part weight. Also, the tensile test recorded mechanical investigations such as elongation at break and maximum failure load. It should also be noted that the programmed weight, after determining the geometric parameters (number of contours, layer thickness and its overlap percentage and core density) was determined by the software.

Figure 3 is shown the FDM printed specimens after the universal testing machine. Since the tensile strength of the fibres is greater than the strength and adhesion between them, with the loading of the specimen, the fibres tend to change direction in the loading direction, and the more the fibres are in the tensile direction, the elongation at break for the specimen increases [54,55]. Based on extension - force diagrams of two types of failure, ductile (sample # 14) and brittle specimen (sample # 8), are shown in Figure 4. Sample 8 and 14 have the same printing speed and number of contours (5). Sample 8 has a lower layer thickness (0.2 mm) and infill density (25%), which, as

expected, has a lower density (increase in empty space), a decrease in mechanical properties, and a lower layer thickness at the same printing speed, increases the cooling rate, which causes more brittleness, so it can be said that the sample 8 is more brittle due to lower density and faster cooling rate compared to sample 14.

Figure. 3. fracture of the specimen after tensile test

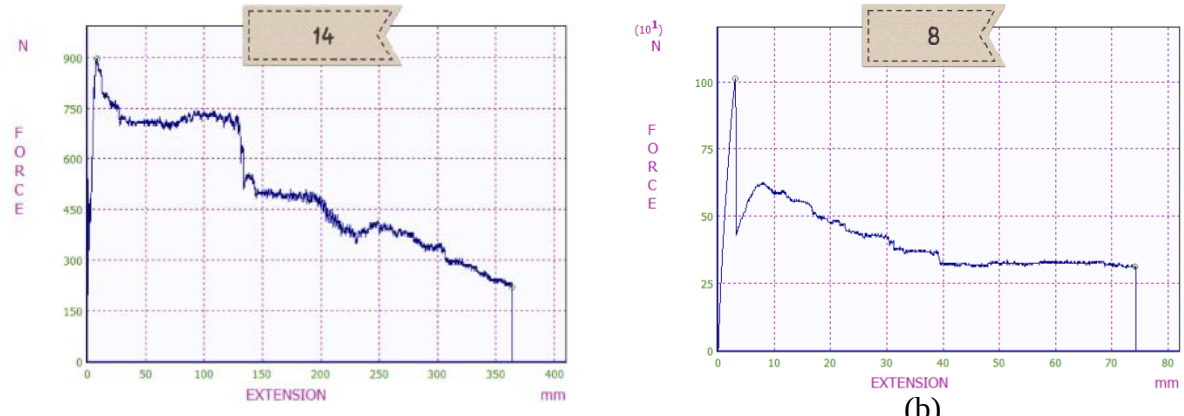

(a) (b)

Figure. 4. Extension-Force diagrams of (a) ductile specimen (sample # 14) and (b) brittle specimen (sample # 8)

3. Results and Discussion

In statistical science, analysis of variance (ANOVA) is an significant method to analysis of statistical models and their interaction estimation procedures in the analysis of experimental data [36]. Based on process condition, a multi factor ANOVA is appropriated in this study. The factors can be estimated as a part of this ANOVA test in the both effects and interactions. In that case, the design is crossed, not nested, and the premise that factors are fixed, not random. In this approach, some terms such as p-values, lack of fit, and R-squared values for comparing models are crucial for defining the interaction and influence of process parameters. F-values imply that these models can be used to study the design space, and models are desirable. As Design-Expert^{TM} software offers a guideline to select a correct power law transformation, the software selects higher polynomial where additional terms are significant, and the model is not aliased.

3.1 Maximum Failure Load

To define the influence of the process parameters as well as the regression model were extracted based on response surface analysis. The results of the analysis of variance are given in Table 6. In the analysis of variance, the alpha value in F-value is considered to be 0.05, which indicates that if the probability of P in the analysis of variance is less than 0.05, the relevant parameter with a probability of more than 95% is effective. Also, the value of R-Sq=88.5% and R-Sq (adj) =73.83%, which indicates the good accuracy of modeling by RSM. Figurer 5 indicates the normal probability plot of the residuals during the failure. The normal probability plot illustrates whether residuals follow a normal scattering; in this case, the points follow a straight line. However, some moderate scatter even with normal data is expected.

According to the analysis of variance table (table 6), it could be concluded that the parameter of the number of contours (C-20.86%), second power of contours number (C^2-30.35%) and the interaction of the number of contours and the thickness of the layer (AC-19.75%) are affected the maximum amount of force during failure. The effectiveness of the second power components of the parameters confirms the secondary model. Based on the regression analysis and removing the ineffective parameters, the mathematical equation in order to predict the maximum force during the polymer failure is extracted.

Table 6. Analysis of variance (ANOVA) for maximum failure load

Source	Sum of Squares	Degree of freedom	Mean square	F-value	P-value	Percentage contribution %
Model	56206.08	9	6245.12	6.02	0.01370	-
A-LT	4896.50	1	4896.50	4.72	0.0664	7.71
B-IP	31.64	1	31.64	0.0305	0.8664	0.04
C-NC	13242.26	1	13242.26	12.76	0.0091	20.86
AB	2342.70	1	2342.70	2.62	0.1767	3.69
AC	12537.36	1	12537.36	12.08	0.0103	19.75
BC	3591.28	1	3591.28	3.46	0.1052	5.65
A^2	4295.59	1	4295.59	4.14	0.0814	6.76
B^2	4746.73	1	4746.73	4.57	0.0698	7.47
C^2	19270.08	1	19270.08	18.56	0.0035	30.35
Residual	7267.03	7	1038.15		0	
Lack of Fit	7267.03	5	1453.41	50.18	0.0197	
Pure Error	0.0000	2	0.0000			
Total	63473.11	16				
R-Squared= 88.55%			R-Squared (Adj)= 73.83%			

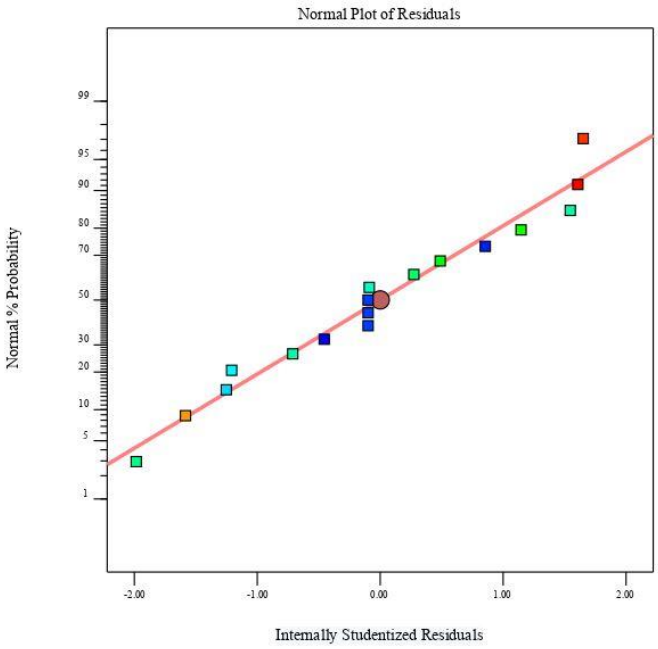

Figure 5. The normal plot of residuals of failure load

To make estimates about the response for given levels of each factor equation in terms of coded factors can be used. Also, in order to identify the relative impact of the factors by comparing the factor coefficients the coded equation is useful. Elongation at break in terms of coded factors is calculated by following equation:

Maximum failure load (N) =137.54-17.49 LT+1.41 IP +28.77 NC -39.59 LT*NC+31.54 NC^2 (1)

Equation (2) is predictive model of maximum failure load in terms of actual values (significant parameter):

Maximum failure load (N) = 978.11-1359.22LT-27.849IP-99.78NC-791.75LT*NC+31.54 NC^2 (2)

The perturbation plot of maximum failure load is shown in figurer 6. By doing so, the effect of all factors in the central point in the design space could be compared. In figure 6 by changing one

parameter over its range while holding other factors constant. According to the Curves A, B, and C, the layer thickness, infill percentage, and number of contour have the maximum impact on maximum failure load, respectively.

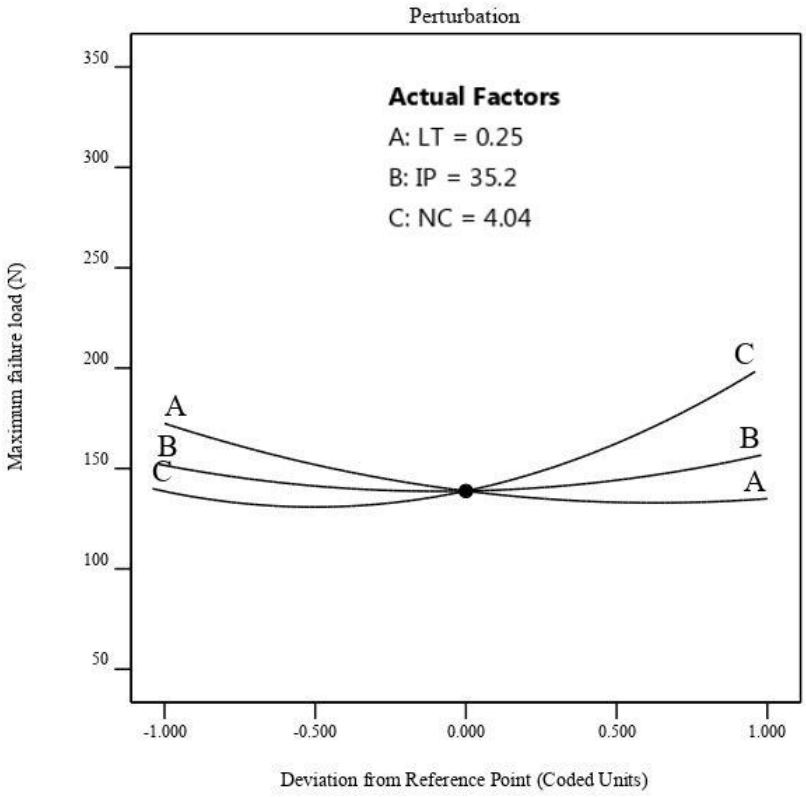

Figure 6. Perturbation plot of maximum failure load

Figurer 6 confirms the results of the ANOVA table and the regression equation. The rate of the regression coded equation shows the effect of different parameters. According to the Figurer 6 and Equation 1, it is clear that the Infill percentage has slight impact on the maximum failure force. The thickness of the layer has a greater impact on the maximum fracture force than the infill percentage. According to Figurer 6, it is clear that the maximum failure force occurs at a layer thickness of 0.2. Based on Figurer 6, the maximum amount of refractive power decreases with increasing layer thickness.

As shown in Figure 6 by increasing the thickness of the layer from 0.15 mm to 0.35 mm, the maximum failure load is decreased from 172 N to 134 N and the failure rate has significant reduced (22%). Based on the literature [33,36], once the thickness of the layer increasing, amount of failure force will be increased. However, in the case of nylon, different results have been obtained. As a result, by increasing the thickness of the layer, the number of layers will be increased.

In order to achieve the appropriate fusion, the plate temperature should be adequate, and also the extruder temperature should be high. In this condition, the previous layer is cool enough and a new layer is formed on it and proper inter-layer penetration takes place. Also, the possibility of void formation or lack of inter-layer adhesion is reduced. In fact, the formation of voids and the lack of proper penetration as well as adhesion is reduced the strength of the sample against tensile loads.

According to the results, it is clear that in the samples of polyamide tensile test, the interlayer connection process has been done well. Indeed, the device canning speed also greatly effects on the adhesion of the layers during the process. In this study, the print speed was set on 3600 mm/min. By doing so, due to reduce the speed of the deposition, the cooling rate transition is irregulated, and as a result, good adhesion between the layers is not formed.

In other scenario, by increasing the layer thickness, the number of interlayer adhesion paths decreased, and in fact the cross-section of the sample becomes closer to the plastic injection sample. Furthermore, the cross-sectional area of the uniformity is formed, which increases the strength of the specimens. Finally, the maximum force during failure is increased. However, based on the results there is a different scenario. According to the heat transfer rate (equation 3), it is clear that the more area of cross-sectional is, the more heat transfer rate and the cooling rate has occurred. One of the most important points in the layer temperature is lack of proper penetration due to the cooling rate of the previous layers before the new layers are placed. In this lack of proper

adhesion, the possibility of cavity formation increases and these holes are connected together during the tensile test and reduce the resistance of the sample against tensile loads.

$$Q=h\ A\ (T_s-T_b) \quad (3)$$

Due to the process condition, in the large layer cross-section, the temperature of the upper part of the layer and the lower layer is different after the placement on each layer. In fact, by increasing the layer thickness, there is a difference condition between the top layer and the bottom layer. During the bonding of the layers to each other and Colling process, it is possible to create thermal stresses in the layers with greater thickness, which has a negative effect on the material properties during the tensile loads. In the contrast, by reducing the thickness layer the thermal stresses significant reduce between the layers. In this regard, increasing the print bed temperature can partially solve this problem. In addition, the direction of the force applied to the device is also very important in terms of the direction of the layers.

According to Figurer 6, it is clear that the number of contour layers is much more influential than the other parameters evaluated on the maximum failure force. By increasing the number of contour layers from 2 to 6, the maximum force in failure increased 42%. In addition, the direction of the contour layers, which is formed as rectangle pattern around the sample, greatly affects the rate of increasing. The layers generated in these samples are in the direction of the tensile force during tensile test. The alignment of these lines with the direction of the applied force causes the overlap of the layers with each other whereas increases the strength of the samples by increasing the number of layers.

Here, since the force is applied in line with the direction of the layer, the high strength properties of the polyamide have significant effect. In fact, the possibility of expansion of cavities is

decreased with respect to the direction of the applied force. Also, appropriate overlap between the outer layers and the internal structure is also effective on this phenomenon. In this current study almost 15% overlap has been considered. Interestingly, there is a correlation relation between solidity of the printed parts and infill percentage, however, has less impact on the strength of parts which somewhat associated to the solid surface of samples. Figurer 7 shows the 3D surface plot of maximum failure load in terms of number of contour and layer thickness.

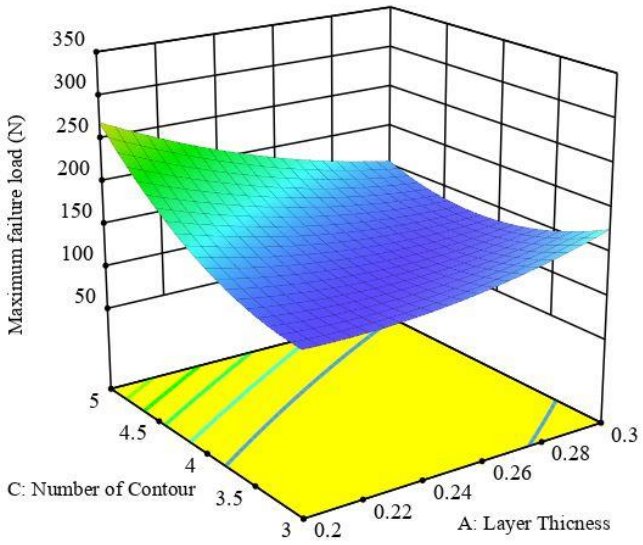

Figure 7. 3D surface plot of maximum failure load in terms of number of contour and layer thickness.

Based on Figurer 7, in the minimum number of layers, with increasing layer thickness, the maximum failure force is increased. Beside, in a large number of contours, by increasing the thickness of the layer the maximum amount of failure force is reduced. According to Figure 7, the maximum failure force occurred at the maximum number of contours and at the lowest layer thickness.

3.2 Elongation at Break

The effect of layer thickness, infill percentage and number of contours on Elongation at break during failure is the second variable is studied. In this regard, Table 7 shows the results of the analysis of variance for elongation at break. Due to the enormous effect of the second power of the parameters, a second-order model has been proposed to predict the values of Elongation at break. Obviously, based on table the model, which indicates good modeling accuracy by surface response method, R-Sq = 74% and R-Sq (adj) = 42%. Also, the normal distribution diagram of the residues (Figure 9) also shows the adequacy of the model.

Table 7. Analysis of variance (ANOVA) for Elongation at Break

Source	Sum of Squares	Degree of freedom	Mean square	F-value	P-value	Percentage contribution %
Model	3.483E+05	9	38700.05	2.29	0.1434	-
A-LT	63947.54	1	63947.54	3.79	0.0927	13.70
B-IP	163.03	1	163.03	0.0097	0.9245	0.03
C-NC	30415.01	1	30415.01	1.80	0.2214	6.51
A×B	42276.50	1	42276.50	2.50	0.1576	9.06
A×C	2436.86	1	2436.86	0.1443	0.7153	0.52
B×C	65768.03	1	65768.03	3.90	0.0890	14.09
A^2	63910.97	1	63910.97	3.79	0.0928	13.70
B^2	3442.50	1	3442.50	0.2039	0.6653	0.73
C^2	1.111E+05	1	1.111E+05	6.58	0.0373	23.81
Residual	1.182E+05	7	16883.85			
Lack of Fit	1.182E+05	5	23637.38	50.18	0.0197	
Pure Error	1.464E-003	2	7.320E-004			
Total	4.665E+05	16				
R-Squared= %74			R-Squared (Adj)= %42			

In the current analysis variance, if the alpha value in the F test is considered to be 0.05, none of the parameters are effective. In that case, the alpha level was considered to be 0.1. This indicates

that the layer thickness is effective with a probability of more than 99%. Based on the ANOVA table (table 6), second power of contour number (C^2-23.81%) and multiplication of infill percentage and number of contour (B×C-14.09%) have the grate impact on elongation at break. Equation (4) represents predictive model of elongation at break in terms of coded factors:

Elongation at break (%) =131.08+63.22LT-3.19IN-43.6NC+90.67(IN*NC) +75.33 NC² (4)

Equation (5) represents predictive model of elongation at break in terms of actual values:

Elongation at break (%) = 5004.12-13916LT-82.26IP-879.3NC+9.06IP*NC+75.73 NC² (5)

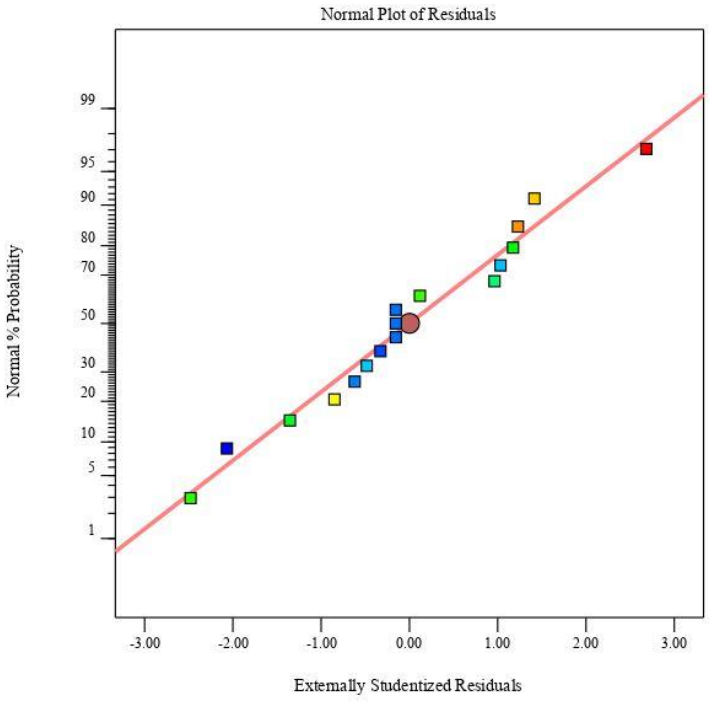

Figure 8. The normal plot of residuals of Elongation at Break

The perturbation plot of elongation at break is shown in figurer 8. In that case, Lines A, B, and C show sensitivity of elongation at break to the layer thickness, infill percentage, and number of contour, respectively.

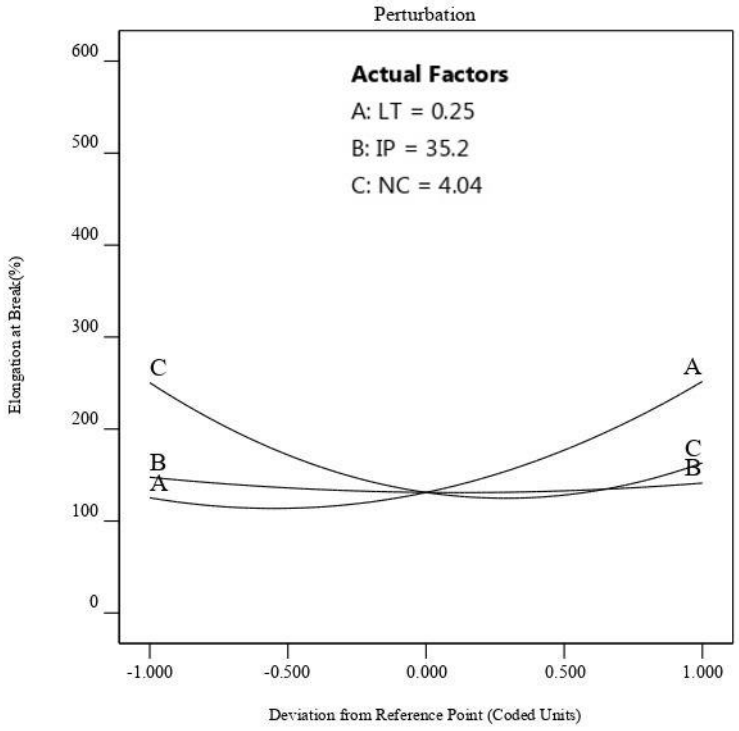

Figure 8. Perturbation plot of elongation at break

Base on the results, infill percentage has the same impact in the elongation at break and maximum force in the failure. In this study, honeycomb strategy was used for infill pattern, and density of the pattern is defined by infill percentage. Based on the honeycomb geometry, it can facilitate the redistribution of localized stresses to endure stress concentrations to undergo more plastic deformation when the infill percentage is maximum. Generally, the infill percentage does not have much effect on the elongation during failure. In the contrast, the effect of layer thickness on the elongation is greater than the effect of this parameter on the maximum force during failure. As a

result, by increasing the layer thickness from 0.15 to 0.55, the elongation at break increased from 125% to 251%. Therefore, increasing layer thickness directly results in less interlayer adhesion.

Additionally, it could be concluded that the cross-sectional area of the sample is more uniform, and for a constant force, the increment will be longer before failure. It realized form Figurer 8 that increasing the number of contour, increased the maximum force of failure, while reduced the elongation at failure. One of the most outstanding points in FDM parts is the relationship between the mechanical properties and interlayer solidarity of plastic strings. Due to the process condition, the extruder puts a string on a layer which is already cooled down to a remarkable lower temperature than the temperature of the extruded string. The difference in temperatures for each layer will cause strings to not fuse thoroughly together. Also, the most common defects in FDM, warping, occurred in this period of time. The print cool at different rates, section's sizes also change at diverse speeds. Once strings do not fuse perfectly, it is rational to suppose that the part will have a brittle fracture and also various cooling rate causes the buildup of interior stresses that pull the underlying layer upwards. Consequently, in the manufacture of samples with minimum infill percentage, there is less time to heat transfer and less difference in temperatures which ends in better interlayer adhesion between plastic strings. It is realized from Figure 9 that the maximum elongation at break is occurred on 25% and 3 in the infill percentage and number of contour, respectively.

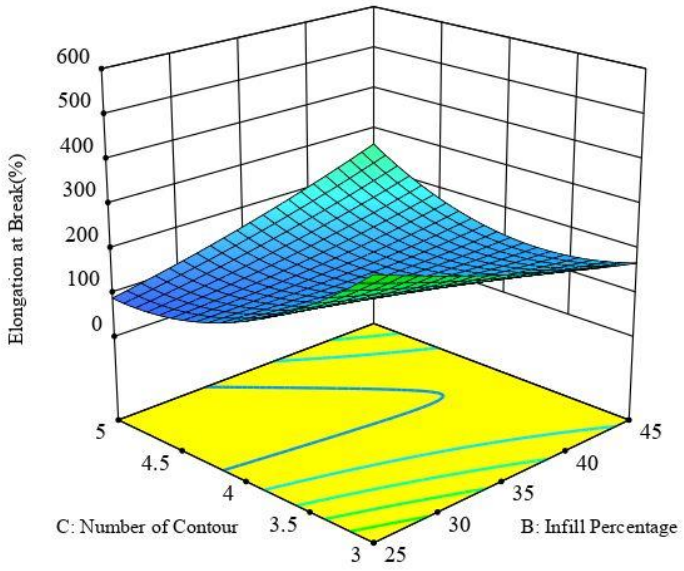

Figure 9. 3D surface plot of Elongation at Break in terms of layer thickness and number of contour.

3.3 Part Weight

The parts weight is examined as the third output is investigated. Parts weight deviation is one of the most frequent sources of counting errors. To this end, in this study nylon was used as the filament material in order to achieve the lightweight structures. To improve stiffness/weight ratios and increase mechanical properties nylon is also frequently filled with glass fibers or mineral. Thus, this makes it one of the common and strongest and polymer offered at AM technology. Due to the material characterization it is self-lubricating, very wear-resistant and thermally stable is an excellent candidate for rotary equipment and medical application. In addition, very light, with 15% the weight of steel and 40% of aluminum.

The information obtained from the analysis of variance is given in Table 8. The p-value values of the ANOVA table indicate that the layer thickness, infill percentage and number of

contours affect the sample weight. The proposed model of design expert software to predict the weight of samples is a completely linear model.

Table 8. Analysis of variance (ANOVA) for part weight

Source	Sum of Squares	Degree of freedom	Mean square	F-value	P-value	Contribution percentage %
Model	2,05	3	0.6823	32.62	< 0.0001	Significant
A-LT	0.7656	1	0.7656	36.60	< 0.0001	33
B-IP	0.6006	1	0.6006	28.71	0.0001	25.88
C-NC	0.6806	1	0.6806	32.54	< 0.0001	29.33
Residual	0.2719	13	0.0209			
Lack of Fit	0.2719	11	0.0247			
Pure Error	0.0000	2	0.0000			
Total	2.32	16				
R-Squared= %8827			R-Squared (Adj)= %8557			

Equation 6 expresses predictive model of part weight in terms of coded factors:

Part weight (gr) =3.86+0.2188LT+0.1938IP+0.2063NC (6)

Equation 7 expresses predictive model of part weight in terms of actual values:

Part weight (gr) =1.2678+4.3LT+0.019IP+0.2062NC (7)

Based on the equations, it could conclude that the effect of the parameters on the weight of the sample is relatively the same. Figurer 10 shows the effect of different parameters on the sample weight. The slope of the lines in the Figurer also confirms the effect of the parameters and linear relationship.

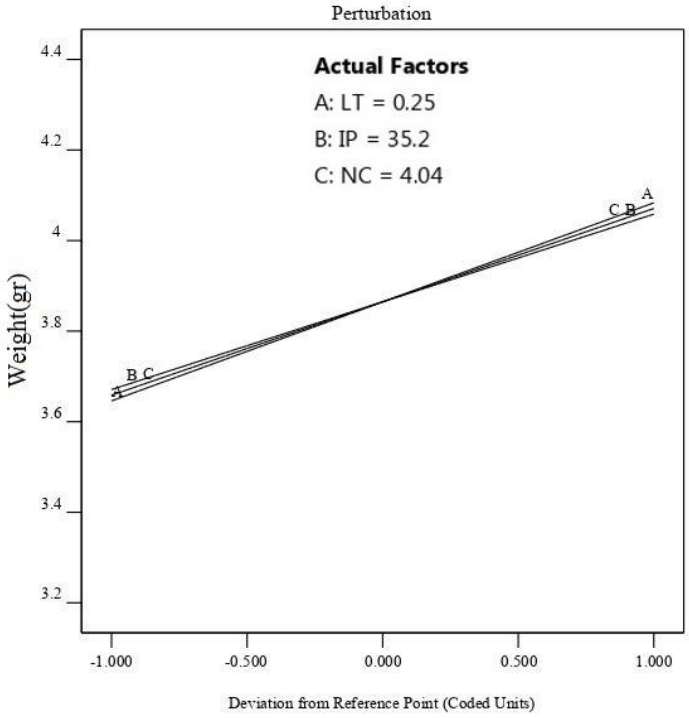

Figure 10. Perturbation plot of part weight

It is realized from Figurer 10 that by increasing the thickness of the layer, the infill percentage as well as the number of contours the weight of the samples increased. Based on equations and the slope of the lines, the infill percentage has the minimum impact than others.

Based on the tensile test specimen dimension, honeycomb internal pattern contains a slight portion of the specimen. Actually, this internal portion would be greater impact in larger manufacturing.

3.4 Build Time

Nowadays, one of the most critical aspect in manufacturing science, especially in mass production is estimate of build time. In this current study, build time is considered as an objective function. Figurer 11 indicates the normal probability plot of the residuals during the failure. The normal probability plot indicates whether residuals follow a normal distribution; in this case, the points follow a straight line. Some moderate scatter even with normal data is expected.

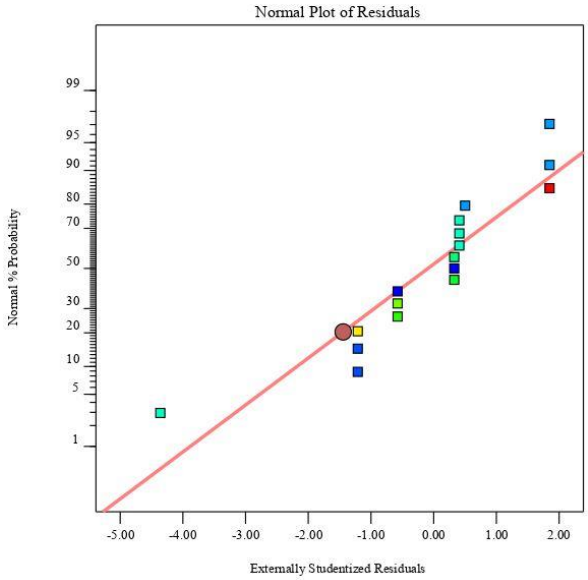

Figure 11. The normal plot of residuals of built time.

As shown in table 9, thickness, infill percentage and number of contour are most important controlled variables for the build time. Furthermore, the square of layer thickness has a major effect on build time. Build time in terms of coded factors are shown in Equation 8:

Build time (min) =19.87-3.19LT-+0.8125IN+1.06NC-0.3750(IN*NC)-0.625(LT*NC) +0.60 LT^2 (8)

Equation 9 is predictive model of build time in terms of actual values:

Build time (min) =21.12-109.2LT+0.41IP+4.7NC-0.75LT*IP-12,5LT*NC+243.4 LT^2 (9)

Table 9. Analysis of variance (ANOVA) for build time

Source	Sum of Squares	Degree of freedom	Mean square	F-value	P-value	Percentage contribution %
Model	206.63	9	22.96	178.68	< 0.0001	Significant
A-LT	162.56	1	162.56	1265.14	< 0.0001	78.33
B-IP	10.56	1	10.56	82.20	< 0.0001	5.08
C-NC	18.06	1	18.06	140.57	< 0.0001	8.70
A×B	1.13	1	1.13	8.76	0.0211	0.54
A×C	3.13	1	3.13	24.32	0.0017	1.50
B×C	0.1250	1	0.1250	0.9728	0.3568	0.06
A^2	7.18	1	7.18	55.85	0.0001	3.45
B^2	0.3867	1	0.3867	3.01	0.1264	0.18
C^2	0.0051	1	0.0051	0.0401	0.8470	0.002
Residual	0.8995	7	0.1285			
Lack of Fit	0.8995	5	0.1799			
Pure Error	.0000	2	.0000			
Total	207.53	16				
R-Squared= 99.57%			R-Squared (Adj)= 99.01%			

According to the high values of R-Squared and adjusted R-Squared the predictive model is still reliable. Based on the equations, the layer thickness coefficient is higher than infill percentage coefficient. Figure 12 is illustrated the perturbation plot of build time. It could be concluded that the layer thickness has a great impact on build time. On the other hand, the build time decreased meaningfully by increasing layer thickness and increased slightly by increasing infill percentage. It can be explained that the build time is immensely affected by layer thickness because by increasing layer thickness the slicer software divides part thickness into fewer sections.

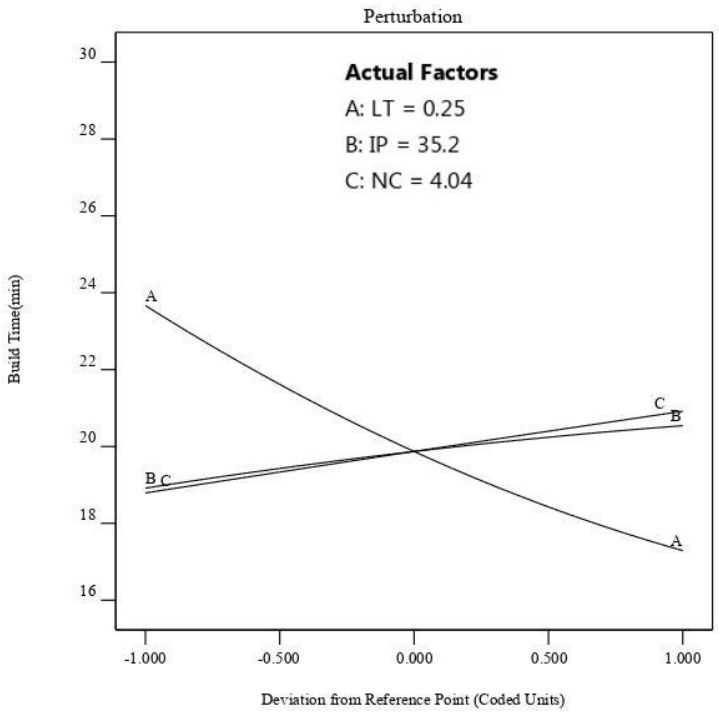

Figure 12. Perturbation plot of build time

Moreover, the nozzle should scan more internal honeycomb pattern lines at defined sections which takes more time by increasing infill percentage. The effects of layer thickness and infill percentage on build time is presented in Figure 13.

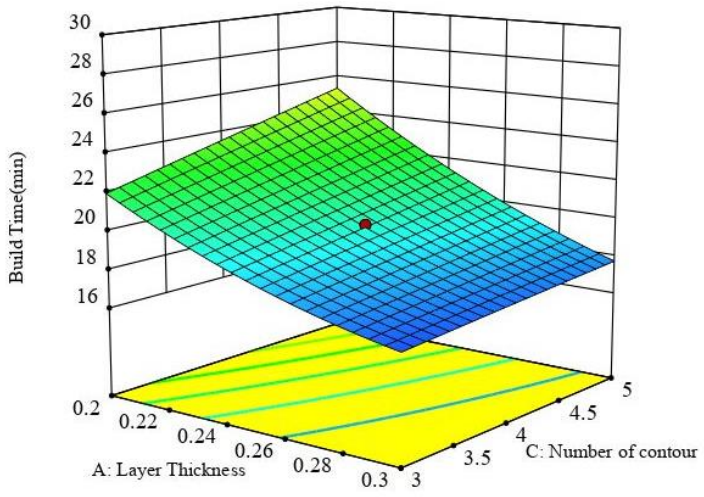

Figure 13. 3D surface plot of build time in terms of layer thickness and Number of contour

Conclusion:

In the present study, nylon 12 tensile test sample was used to study effects of infill percentage, layer thickness, number of contour and their interactions on mechanical properties, build time, and part weight by design of experiment (DOE) method. Due to the importance of optimization in manufacturing science finding the critical condition to prevent the catastrophic failures is absolutely required. The concluding remarks of this study are as follows:

1- One of the significant advantages of FDM process is a fast and cheap operation among AM techniques. Based on the perturbation analysis, the layer thickness and number of contours has a great impact on the build time. Generally, the build time increased slightly by increasing infill percentage and reduced incredibly with increasing layer thickness.

2- The number of contours and infill density had a similar effect on mechanical properties and manufacturing time, because with increasing the number of contours, the part weight increases which results in improvement of the mechanical properties, and on the other hand rises the production time.

3- Experimental results showed that in the same printing conditions, the maximum values of failure load (533 N) and elongation (595.5%) were obtained by changing the layer thickness from 0.2 mm to 0.3 mm. By reduction in layer thickness at the same printing speed, the cooling rate increases, which greatly increases the strength and reduces the elongation. Also, the layer thickness has a definite and decisive effect on the printing time.

4- There was a good agreement between experimental results and RSM predictions, which confirmed the predictive models' reliability. Based on the ANOVA, by increasing the layer thickness from 0.15 to 0.55, the elongation at break increased from 125% to 251%.

References:

[1] Wojtyła S, Klama P, Baran T. Is 3D printing safe ? Analysis of the thermal treatment of thermoplastics : ABS , PLA , PET , and 2017;9624. doi:10.1080/15459624.2017.1285489.

[2] Singh S, Ramakrishna S, Singh R. Material issues in additive manufacturing : A review. J Manuf Process 2017;25:185–200. doi:10.1016/j.jmapro.2016.11.006.

[3] Ngo TD, Kashani A, Imbalzano G, Nguyen KTQ, Hui D. Additive manufacturing (3D printing): A review of materials , methods , applications and challenges. Compos Part B 2018;143:172–96. doi:10.1016/j.compositesb.2018.02.012.

[4] Bhatt PM, Kabir AM, Peralta M, Bruck HA, Gupta SK. A robotic cell for performing sheet lamination-based additive manufacturing. Addit Manuf 2019;27:278–89.

[5] Peverini OA, Addamo G, Lumia M, Virone G, Calignano F, Lorusso M, et al. Additive manufacturing of Ku/K-band waveguide filters: A comparative analysis among selective-laser melting and stereo-lithography. IET Microwaves, Antennas Propag 2017;11:1936–42.

[6] Paul R, Anand S. Process energy analysis and optimization in selective laser sintering. J Manuf Syst 2012;31:429–37.

[7] Abedi HR, Hanzaki AZ, Azami M, Kahnooji M, Rahmatabadi D. The high temperature flow behavior of additively manufactured Inconel 625 superalloy. Mater Res Express 2019;6:116514. doi:10.1088/2053-1591/ab44f6.

[8] Patil AS, Hiwarkar VD, Verma PK, Khatirkar RK. Effect of TiB2 addition on the microstructure and wear resistance of Ti-6Al-4V alloy fabricated through direct metal laser sintering (DMLS). J Alloys Compd 2019;777:165–73.

[9] Vithani K, Goyanes A, Jannin V, Basit AW, Gaisford S, Boyd BJ. An overview of 3D printing technologies for soft materials and potential opportunities for lipid-based drug delivery systems. Pharm Res 2019;36:4.

[10] Kerekes TW, Lim H, Joe WY, Yun GJ. Characterization of process--deformation/damage property relationship of fused deposition modeling (FDM) 3D-printed specimens. Addit Manuf 2019;25:532–44.

[11] Daminabo SC, Goel S, Grammatikos SA, Nezhad HY, Thakur VK. Fused deposition modeling-based additive manufacturing (3D printing): techniques for polymer material systems. Mater Today Chem 2020;16:100248. doi:10.1016/j.mtchem.2020.100248.

[12] Access O. 3D printing of textile-based structures by Fused Deposition Modelling (FDM) with different polymer materials 3D printing of textile-based structures by Fused Deposition Modelling (FDM) with different polymer materials 2014. doi:10.1088/1757-899X/62/1/012018.

[13] Stansbury JW, Idacavage MJ. 3D printing with polymers : Challenges among expanding options and opportunities. Dent Mater 2015;32:54–64. doi:10.1016/j.dental.2015.09.018.

[14] Wang X, Jiang M, Zhou Z, Gou J, Hui D. 3D printing of polymer matrix composites: A

review and prospective. Compos Part B Eng 2017;110:442–58. doi:10.1016/j.compositesb.2016.11.034.

[15] Sun Q. Effect of processing conditions on the bonding quality of FDM polymer filaments 2008;2:72–80. doi:10.1108/13552540810862028.

[16] Berman B, Zarb FG, Hall W. 3-D printing : The new industrial revolution. Bus Horiz 2012;55:155–62. doi:10.1016/j.bushor.2011.11.003.

[17] Martínez J, Diéguez JL, Pereira A, Pérez JA. Modelization of Surface Roughness in FDM Parts 2012;856:849–56. doi:10.1063/1.4707643.

[18] Dong G, Wijaya G, Tang Y, Zhao YF. Optimizing process parameters of fused deposition modeling by Taguchi method for the fabrication of lattice structures. Addit Manuf 2018;19:62–72. doi:10.1016/j.addma.2017.11.004.

[19] Mahmood S, Qureshi AJ, Talamona D. Taguchi based process optimization for dimension and tolerance control for fused deposition modelling. Addit Manuf 2018. doi:10.1016/j.addma.2018.03.009.

[20] Mohanty AK. Improving the Impact Strength and Heat Resistance of 3D Printed Models: Structure, Property, and Processing Correlationships during Fused Deposition Modeling (FDM) of Poly(Lactic Acid) 2018. doi:10.1021/acsomega.8b00129.

[21] Liu X, Zhang M, Li S, Si L, Peng J, Hu Y. Mechanical property parametric appraisal of fused deposition modeling parts based on the gray Taguchi method. Int J Adv Manuf Technol 2016. doi:10.1007/s00170-016-9263-3.

[22] Moradi M, Meiabadi S, Kaplan A. 3D Printed Parts with Honeycomb Internal Pattern by Fused Deposition Modelling; Experimental Characterization and Production Optimization. Met Mater Int 2019;25:1312–25. doi:10.1007/s12540-019-00272-9.

[23] Moradi M, Aminzadeh A, Rahmatabadi D, Hakimi A. Experimental investigation on mechanical characterization of 3D printed PLA produced by fused deposition modeling (FDM). Mater Res Express 2021. doi:10.1088/2053-1591/abe8f3.

[24] Zhang Y, Purssell C, Mao K, Leigh S. A physical investigation of wear and thermal characteristics of 3D printed nylon spur gears. Tribol Int 2020;141:105953. doi:10.1016/j.triboint.2019.105953.

[25] Chou C, Couch J, Garside N, Banna AH, Junot J, Nelson J, et al. Fused-Deposition Modeling Raster Parameter Effectson Mechanical Properties of Taulman Bridge Nylon 2017:1–20. doi:10.13140/RG.2.2.29215.46241.

[26] Lee J, An J, Chua CK. Fundamentals and applications of 3D printing for novel materials. Appl Mater Today 2017;7:120–33. doi:10.1016/j.apmt.2017.02.004.

[27] In P. Progress In Electromagnetics Research Letters, Vol. 34, 75–82, 2012 2012;34:75–82.

[28] Dilberoglu UM, Gharehpapagh B, Yaman U, Dolen M. The role of additive manufacturing in the era of Industry 4 . 0. Procedia Manuf 2017;11:545–54.

doi:10.1016/j.promfg.2017.07.148.

[29] Singh R, Singh S. Development of nylon based FDM filament for rapid tooling application. J Inst Eng Ser C 2014;95:103–8.

[30] Sunny SF, Gleason GH, Malik AS. Comparison of numerical methods for fluid-structure interaction simulation of fused deposition modeled nylon components. Procedia Manuf 2019;34:516–27. doi:10.1016/j.promfg.2019.06.215.

[31] Singh R, Singh S. Experimental Investigations for Statistically Controlled Solution of FDM Assisted Nylon6-Al-Al2O3replica Based Investment Casting. Mater Today Proc 2015;2:1876–85. doi:10.1016/j.matpr.2015.07.139.

[32] Mostafa KG, Montemagno C, Qureshi AJ. Strength to cost ratio analysis of FDM Nylon 12 3D Printed Parts. Procedia Manuf 2018;26:753–62. doi:10.1016/j.promfg.2018.07.086.

[33] Moradi M, Moghadam MK, Shamsborhan M, Bodaghi M, Falavandi H. Post-processing of FDM 3d-printed polylactic acid parts by laser beam cutting. Polymers (Basel) 2020;12:550. doi:10.3390/polym12030550.

[34] Nagendra J, Prasad MSG, Shashank S, Vijay N, Suresh V. Nylon-aramid polymer composite as sliding liner for lube-less sliding bearing by fused deposition modeling Nylon-Arami olym r om o i li in arin y a li in in r or o i ion o lin 2019;020047. doi:10.1063/1.5085618.

[35] Nagendra J, Prasad MSG, Shashank S, Md Ali S. Comparison of tribological behavior of nylon aramid polymer composite fabricated by fused deposition modeling and injection molding process. Int J Mech Eng Technol 2018;9:720–8.

[36] Moradi M, Karami Moghadam M, Shamsborhan M, Bodaghi M. The Synergic Effects of FDM 3D Printing Parameters on Mechanical Behaviors of Bronze Poly Lactic Acid Composites. J Compos Sci 2020;4:17. doi:10.3390/jcs4010017.

[37] Prasada VD, Rajiv P, Geethika VN. Materials Today : Proceedings Effect of fused deposition modelling (FDM) process parameters on tensile strength of carbon fibre PLA. Mater Today Proc 2019;18:2012–8. doi:10.1016/j.matpr.2019.06.009.

[38] Constantinou P, Roy S. Experimental investigation on flexural properties of FDM processed Nylon 12 parts using RSM Experimental investigation on flexural properties of FDM processed Nylon 12 parts using RSM 2018. doi:10.1088/1757-899X/377/1/012137.

[39] Vishwas M, Basavaraj CK, Vinyas M. Experimental Investigation using Taguchi Method to Optimize Process Parameters of Fused Deposition Modeling for ABS and Nylon Materials. Mater. Today Proc., vol. 5, Elsevier Ltd; 2018, p. 7106–14. doi:10.1016/j.matpr.2017.11.375.

[40] Kumar S, Ranjeet P, Sahu K. Optimization of fused deposition modeling process parameters using a fuzzy inference system coupled with Taguchi philosophy. Adv Manuf 2017. doi:10.1007/s40436-017-0187-4.

[41] Caminero MA, Caminero MA. NU 2017. doi:10.1016/j.matdes.2017.03.065.

[42] Moradi M, Abdollahi H. Statistical modelling and optimization of the laser percussion microdrilling of thin sheet stainless steel. Lasers Eng 2018;40:375–93.

[43] Safari M, Alves de Sousa R, Joudaki J. Fabrication of Saddle-Shaped Surfaces by a Laser Forming Process: An Experimental and Statistical Investigation. Metals (Basel) 2020;10:883. doi:10.3390/met10070883.

[44] Aminzadeh A, Parvizi A, Moradi M. Multi-objective topology optimization of deep drawing dissimilar tailor laser welded blanks; experimental and finite element investigation. Opt Laser Technol 2020;125. doi:10.1016/j.optlastec.2019.106029.

[45] Moradi M, KaramiMoghadam M. High power diode laser surface hardening of AISI 4130; statistical modelling and optimization. Opt Laser Technol 2019;111:554–70. doi:10.1016/j.optlastec.2018.10.043.

[46] Moradi M, Salimi N, Ghoreishi M, Abdollahi H, Shamsborhan M, Frostevarg J, et al. mass balance Parameter dependencies in laser hybrid arc welding by design of experiments and by a mass balance 2014;022004. doi:10.2351/1.4866675.

[47] Moradi M, Arabi H, Shamsborhan M. Multi-objective optimization of high power diode laser surface hardening process of AISI 410 by means of RSM and desirability approach. Optik (Stuttg) 2020;202:163619. doi:10.1016/j.ijleo.2019.163619.

[48] Giovanni M. Response surface methodology and product optimization. Food Technol 1983.

[49] Safari M, Hamidipour • S, Elahi • S H, Tahmasbi • V. Creep Age Forming of Aluminum 7075 Tailor-Machined Blanks: Statistical Modeling, Sensitivity Analysis and Multi-objective Optimization. Trans Indian Inst Met n.d.;73. doi:10.1007/s12666-019-01836-4.

[50] Safari M, Mostaan H, Yadegari Kh H, Asgari D. Effects of process parameters on tensile-shear strength and failure mode of resistance spot welds of AISI 201 stainless steel n.d. doi:10.1007/s00170-016-9222-z.

[51] Mäkelä M. Experimental design and response surface methodology in energy applications: A tutorial review. Energy Convers Manag 2017;151:630–40. doi:10.1016/j.enconman.2017.09.021.

[52] Mago J, Kumar R, Agrawal R, Singh A, Srivastava V. Modeling of Linear Shrinkage in PLA Parts Fabricated by 3D Printing Using TOPSIS Method. Adv. Addit. Manuf. Join., Springer; 2020, p. 267–76. doi:10.1007/978-981-32-9433-2_23.

[53] ASTM C. ASTM Standards, 1958.

[54] Kiendl J, Gao C. Controlling toughness and strength of FDM 3D-printed PLA components through the raster layup. Compos Part B Eng 2020;180:107562. doi:10.1016/j.compositesb.2019.107562.

[55] Mohamed OA, Masood SH, Bhowmik JL. Experimental investigation of time-dependent mechanical properties of PC-ABS prototypes processed by FDM additive manufacturing process. Mater Lett 2017;193:58–62.